Imaging of Vascular Wall Fine Structure in the Human Retina Using Adaptive Optics Scanning Laser Ophthalmoscopy

Toco Y. P. Chui, Thomas J. Gast, and Stephen A. Burns

School of Optometry, Indiana University, Bloomington, Indiana

Correspondence: Stephen A. Burns, School of Optometry, Indiana University, 800 E. Atwater Avenue, Bloomington, IN 47405-3860; staburns@indiana.edu.

Submitted: August 9, 2013
Accepted: September 17, 2013

Citation: Chui TYP, Gast TJ, Burns SA. Imaging of vascular wall fine structures in the human retina using adaptive optics scanning laser ophthalmoscopy. *Invest Ophthalmol Vis Sci.* 2013;54:7115–7124. DOI: 10.1167/iovs.13-13027

Purpose. To improve the ability to image the vascular walls in the living human retina using multiply-scattered light imaging with an adaptive optics scanning laser ophthalmoscope (AOSLO).

Methods. In vivo arteriolar wall imaging was performed on eight healthy subjects using the Indiana AOSLO. Noninvasive imaging of vascular mural cells and wall structure were performed using systematic control of the position of a 10× Airy disk confocal aperture. Retinal arteries and arterioles were divided into four groups based on their lumen diameters (group 1: ≥100 μm; group 2: 50–99 μm; group 3: 10–49 μm; group 4: <10 μm).

Results. Fine structure of retinal vasculature and scattering behavior of erythrocytes were clearly visualized in all eight subjects. In group 1 vessels the mural cells were flatter and formed the outer layer of regularly spaced cells of a two (or more) layered vascular wall. In the vessels of groups 2 and 3, mural cells were visualized as distinct cells lying along the lumen of the blood vessel, resulting in a wall of irregular thickness. Vascular wall components were not readily identified in group 4 vessels.

Conclusions. Our results show that retinal vascular mural cells and wall structure can be readily resolved in healthy subjects using AOSLO with multiply scattered light imaging for retinal vessels with a lumen diameter greater than or equal to 10 μm. Our noninvasive imaging approach allows direct assessment of the cellular structure of the vascular wall in vivo with potential applications in retinal vascular diseases such as diabetes and hypertension.

Keywords: retina, blood vessels, pericytes, endothelial cells, adaptive optics scanning laser ophthalmoscope, dark field imaging

Adaptive optics retinal imaging is an emerging technology for providing high resolution, in vivo imaging of the human retina.[1–7] One of the most striking advancements enabled by adaptive optics imaging has been the ability to visualize individual photoreceptors cells.[8–12] This capability has enabled detailed studies of the spatial distribution of photoreceptors as well as individual variations. These capabilities, in turn, have enabled increasing sophistication in understanding the relation between vision and the photoreceptor matrix.[13–15] Clinically, the ability to quantify both the number and spatial arrangements of the cones has raised the possibility of detailed examination of photoreceptor changes in retinal disease,[16–20] as well as the possibility of improved monitoring of advanced therapies for photoreceptor degenerations.

Recently, adaptive optics scanning laser ophthalmoscopy (AOSLO) has been extending the power of in vivo microscopic imaging to the study of other retinal features, including retinal nerve fiber layer,[21] RPE,[22–24] microvascular mapping,[25–28] and enabling precise measurements of blood flow based on erythrocyte or leukocyte movement.[29–33] Vascular imaging is an especially exciting application area for adaptive optics retinal imaging because there is a strong need for improved biomarkers in ocular as well as systemic vascular disease.[34] Diabetic retinopathy, for example, is a major cause of visual dysfunction in the developed countries.[35] Early diagnosis and treatment of diabetic retinopathy is essential for the prevention of severe visual loss. It is clear from histopathologic studies that the earliest anatomical changes occur with pericyte and endothelial cell apoptosis before any clinical manifestations are present.[36] Changes in retinal vascular wall morphology such as basement membrane thickening, loss of pericytes, and endothelial cells are also well documented in the histopathology of early diabetic retinopathy.[36–38] Although conventional funduscopic assessment and intravenous fluorescein angiography[39] of the retinal vasculature may provide valuable clinical information regarding the state of diabetic retinopathy, their ability to visualize the actual retinal vessels composed of low contrast mural cells as opposed to the contents of the vasculature, is severely impaired by the ocular aberrations of the human eye.

Modern retinal vasculature imaging techniques, such as the retinal function imager,[40] optical coherence tomography (OCT),[41–43] and adaptive optics ophthalmoscopy,[26,28,44,45] are increasingly capable of providing information on the vascular pattern in both healthy and diseased retinas. However, these techniques provide limited visualization of the substructure of the vascular walls. In this paper, we investigated the ability of retinal imaging with an AOSLO combined with a dark field detection scheme[27] to improve the visualization of the vascular

walls with the goal of enabling cellular imaging of the retinal vasculature.

Methods

Subjects

Eight healthy subjects (8 eyes; 7 males and 1 female; age range, 18–58 years, mean ± SD = 32 ± 14) participated in this study. An additional subject (36-year-old male) was imaged to demonstrate the general effect of a large displaced aperture on a perifoveal arteriole (Fig. 1) using our dark field imaging approach.[27] All subjects received a complete eye examination, including a dilated fundus examination. Exclusion criteria included any retinal pathology or systemic diseases such as systemic hypertension. Pupil dilation was achieved with 1 drop of 1% tropicamide. All subjects had best corrected visual acuity of 20/20 or better. A 30° × 30° Infrared scanning laser ophthalmoscopy (SLO) fundus image and 20° × 15° OCT were obtained for each subject using the Spectralis OCT (Heidelberg Engineering, Heidelberg, Germany). Optical coherence tomography data were used as additional exclusion criteria only. Axial length measurement of the tested eye was obtained using an IOL Master (Carl Zeiss Meditec, Dublin, CA). Adaptive optics scanning laser ophthalmoscope imaging was performed on one eye in each subject. Informed consent was obtained after a full explanation of the procedures and consequences of the study. This study protocol was approved by the Indiana University review board and complied with the requirements of the Declaration of Helsinki.

AOSLO Instrumentation

The Indiana AOSLO used in this experiment has been described in detail previously.[46] The Indiana AOSLO uses a supercontinuum source (Fianium Ltd., Southampton, UK) to provide both the wavefront sensing and the infrared imaging sources. Wavefront sensing and infrared imaging were performed at 740 and 820 nm, with wavelengths obtained using interference filters (Semrock, Inc., Lake Forest, IL) with bandwidths of 13 and 12 nm, respectively. Light returning from the retina passes through a confocal aperture optically conjugated to the retinal plane. For the data presented in this paper, this confocal aperture was approximately 10× the Airy disk diameter as measured at the detector plane. Based on theoretical calculations, the axial resolution for this aperture was approximately 150 μm. In this experiment, the vertical and horizontal scanners were programmed to provide full frame images of 1.3° × 1.2° at a frame rate of 28 Hz. Subject's head movements were stabilized using a chin and head rest. The incident corneal power level of the infrared light source was set at 50 μW for the wavefront sensing beacon and 100 μW for the imaging beam. All light levels were safe according to the American National Standards Institute ANSI Z136.[47]

Imaging Retinal Microvasculature Using an Offset Confocal Aperture

The technique for offsetting the confocal aperture and the rationale for using an offset aperture when imaging the retinal vasculature has been described previously.[27] This technique allows us to image the vascular wall fine structure in vivo and noninvasively. In brief the displaced confocal aperture was optically conjugate to the retina, and located in front of the imaging detector. This aperture controls the relative contributions of multiply-scattered[48] and singly-scattered light that forms the retinal image. Typically, displacing the aperture orthogonally to the orientation of the retinal vessel being imaged enhances the visibility of the vascular wall. In this study, the displacement was fixed at 6× the Airy disk diameter horizontally and vertically, depending on the orientation of the targeted blood vessels. This displacement means that no portion of the aperture overlaps the central lobe of the subject's adaptive optics corrected point spread function, ensuring that the images are built up from spatial variations in multiply scattered light. Figure 1 demonstrates the effect of displacing a large confocal aperture on the light return from a 30-μm arteriole located at 5° above the fovea.

Imaging Retinal Arteries and Arterioles With Various Lumen Diameters

Retinal arteries and arterioles with various lumen diameters along the superior or inferior arcade were first marked on the Spectralis SLO en face image before the AOSLO imaging session. Typically, AOSLO imaging was performed along the retinal vascular arcades starting at the superior or inferior optic disc margin. Within the 30-minute imaging session we imaged a number of arterioles to make sure we had all size groups represented for each subject. Retinal arteries and arterioles were then divided into four groups based on their lumen diameters measured on the AOSLO reflectance images after correcting individual retinal magnification factor. Group 1: greater than or equal to 100 μm; group 2: 50 to 99 μm; group 3: 10 to 49 μm (precapillary arterioles); group 4: less than 10 μm. Venules with lumen diameter greater than 100 μm were imaged in all subjects. Venules smaller than 100 μm were imaged occasionally. We avoided cilioretinal arterioles in this study since their origin is anatomically different and pilot studies of cilioretinal arteries showed a thicker, more variable wall structure quite different from that of the retinal arterioles, so this study restricted itself to the usual retinal vessels.

Image Acquisition and Processing

Adaptive optics scanning laser ophthalmoscope images of vascular wall fine structure were recorded as short sections of sequential video frames. A single acquisition of 100 frames (<4 seconds) at each retinal region of interest was sufficient to collect a data set suitable for further image processing. Following acquisition, all video frames were corrected for scan distortion, then the sequence was automatically filtered to reject blinks and large eye movements. A stable video frame was then selected by the program, and all images were aligned to this frame automatically to remove the effect of small eye movements both within and between video frames. Aligned image sequences were used to generate both average images using the lucky averaging approach,[49] and calculations of statistics on a pixel by pixel basis producing the blood vessel perfusion maps.[26] Variations in individual retinal magnification was corrected by taking into account the measured axial length.[10] On the AOSLO reflectance images, individual mural cells were identified as structures with single and focal spatial variations along the blood vessel wall. Mural cell diameter and density along one side of the blood vessel wall were then measured on the AOSLO images manually using a custom MATLAB (The MathWorks, Inc., Natick, MA) program.

Results

The contrast of the vascular walls and associated fine structure was higher for the multiply-scattered light imaging approach with a displaced aperture (Fig. 1B1) when comparing with singly-scattered light imaging approach with a confocal

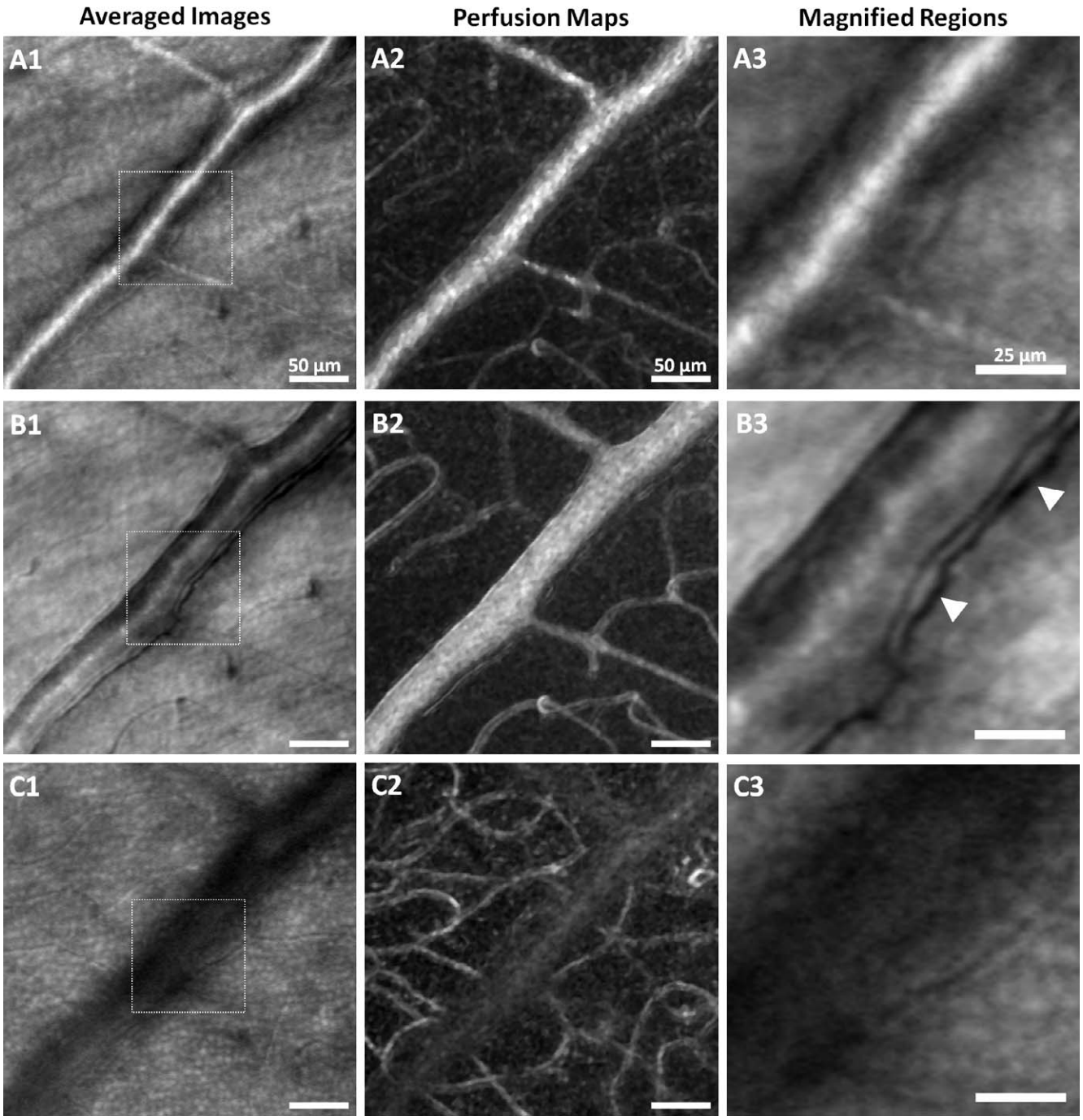

Figure 1. The effect of a large displaced aperture on a 30-μm arteriole located at 5° above the fovea in a 36-year-old male. *Left column* (**A1**, **B1**, **C1**): Averaged AOSLO images. *Middle column* (**A2**, **B2**, **C2**): The vascular perfusion maps of the same regions. *Right column* (**A3**, **B3**, **C3**): The magnified views of the *boxed regions* on the *left column*. (**A3**, **B3**, **C3**) The *rows* illustrate differences arising from differences in imaging conditions. *Top row*: AOSLO images obtained using a large confocal aperture (no displacement) show a strong specular reflection from the retinal nerve fiber layer, masking the microvascular network and the arteriolar wall structure. *Middle row*: The same arteriole, but imaged with a large displaced aperture at the same plane of focus revealing the superficial microvascular network and fine blood vessel wall structure. *Bottom row*: The same arteriole imaged with a large displaced aperture focusing at the deeper retinal layer reveals the deeper microvascular network. *Arrowheads* indicate the vascular mural cells lying along the outer vessel wall. *Scale bars*: 50 μm (**A1**, **A2**, **B1**, **B2**, **C1**, **C2**), 25 μm (**A3**, **B3**, **C3**).

aperture (Fig. 1A1). We were able to image fine structure in the vascular wall in all eight subjects for the vessels of groups 1, 2, and 3 using an AOSLO with a displaced aperture. In general, the best visualization of the arteriolar walls was achieved by displacing the aperture orthogonal to the direction of blood flow.[27] Vascular mural cells are best visualized on one wall due to the asymmetric manner by which we displaced the aperture. The visibility of the walls could be interchanged by changing the direction of offset.

Local specializations of mural cells along the vascular wall in different sizes of blood vessels were seen in all tested subjects. For the large vessels (group 1), the mural cells appeared as elongated structure lying continuously and uniformly along the blood vessel wall (Figs. 2A1, 2A3). Notably,

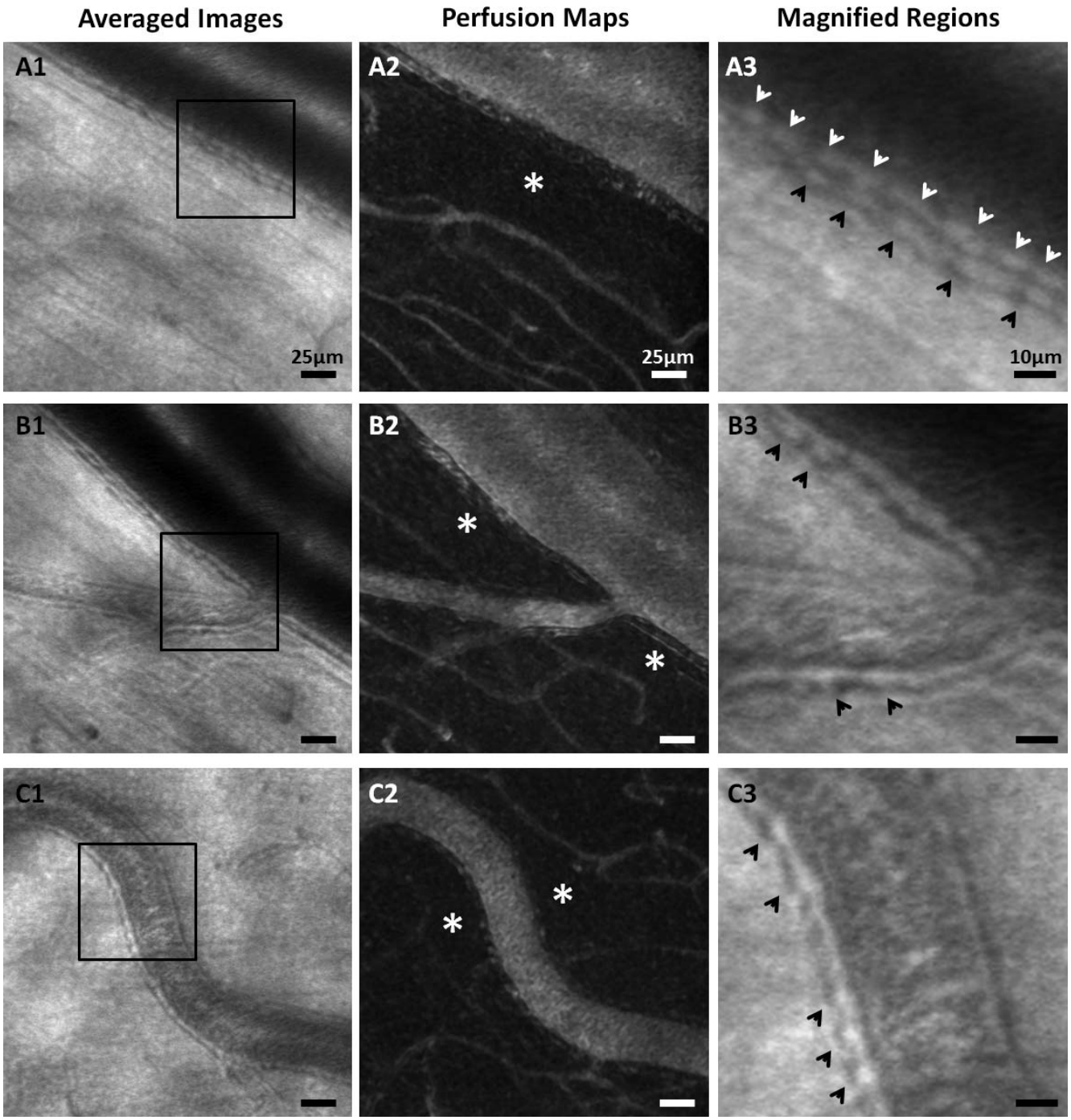

FIGURE 2. Longitudinal cross section of retinal arterioles with lumen diameters of (**A**) 110, (**B**) 90, and (**C**) 30 μm in a 58-year-old male. *Left column* shows the averaged AOSLO images (**A1**, **B1**, **C1**). The corresponding vascular perfusion maps are shown on the *middle column* (**A2**, **B2**, **C2**). *White asterisks* indicate the capillary free zones along the arterioles. *Right column* shows the magnified views of the *boxed regions* on the *left column*. (**A3**, **B3**, **C3**) Fine structure of the arteriolar wall is readily seen in all arterioles including precapillary arterioles. Distinct mural cells are seen along the outer (*black arrows*) and inner (*white arrows*) vessel wall linings. *Scale bars*: 25 μm (**A1**, **A2**, **B1**, **B2**, **C1**, **C2**), 10 μm (**A3**, **B3**, **C3**). Images have been contrast stretched for display purposes.

the vascular wall could be discriminated from the lumen due to the dynamic scattering behavior of erythrocytes in all eight subjects (Supplementary Video S1). For group 2 vessels the cells appeared as rounded structures with a lower packing density (Figs. 2B1, 2B3). Mural cells were also readily identified in group 3 precapillary arterioles as structures bulging outward forming the outer wall surface (Figs. 2C1, 2C3, 3A3, 3B3). The size of the cells as well as the density along the vessels varied with vessel size. The mean (μm) ± SD of mural cells' diameter were 10.9 ± 1.8, 10.4 ± 2.4, and 9.9 ± 1.1 for groups 1, 2, and 3 blood vessels, respectively. The mean ± SD (number of cells/100 μm on one side) of mural cells density was 7 ± 1, 7 ± 3, and 5 ± 2 for groups 1, 2, and 3 blood vessels, respectively. The differences measured were not significantly different for this relatively small sample size. Mural cells of the group 4 vessels were not readily identified with the current

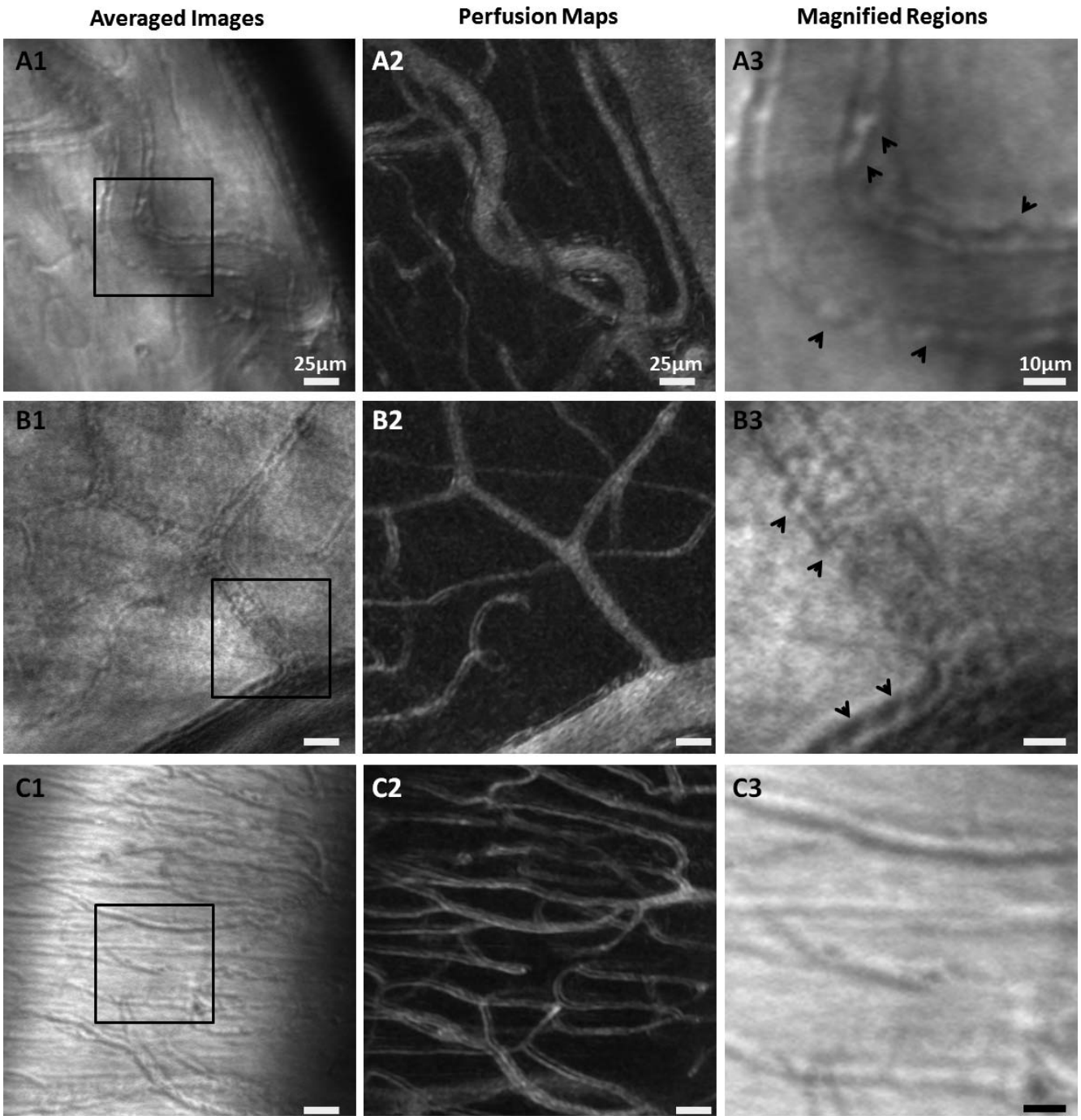

FIGURE 3. Retinal vasculature obtained from three different subjects. The longitudinal cross section of precapillary arterioles with lumen diameters of (**A**) 20 μm, (**B**) 10 μm, and (**C**) capillaries varying between 5 to 8 μm in diameter. *Left column* shows the averaged AOSLO images (**A1**, **B1**) (Supplementary Video S1), and (**C1**) (Supplementary Video S2). The corresponding vascular perfusion maps are shown on the *middle column* (**A2**, **B2**, **C2**). *Right column* shows the magnified views of the *boxed regions* on the *left column*. (**A3**, **B3**, **C3**) Fine structure of the arteriolar wall is seen as cells bulging outward (*black arrows*) forming the outer wall in all precapillary arterioles. Vascular wall components were not identified in retinal capillaries as shown in (**C3**). *Scale bars*: 25 μm (**A1**, **A2**, **B1**, **B2**, **C1**, **C2**), 10 μm (**A3**, **B3**, **C3**). Images have been contrast stretched for display purposes.

imaging approach. Figure 3C3 (Supplementary Video S2) shows group 4 vessels ranging in size from 5 to 8 μm in diameter on the reflectance images. To date, we are not able to identify cellular structures in vessels with a lumen diameter smaller than 10 μm, although occasionally in other pilot studies we have seen some minimal structure in the capillary walls. This point is discussed in more detail later.

In addition to the mural cell appearance, the overall structure of the vascular walls and the surrounding retinal structure also varied with vessel size. In general, group 1 arteriolar walls appeared as three distinct layers as shown in Figure 2A3. As discussed above, the outer lamina showed distinct mural cells (Fig. 2A3, black arrows), which bulged outward, producing a wall of irregular thickness. The inner

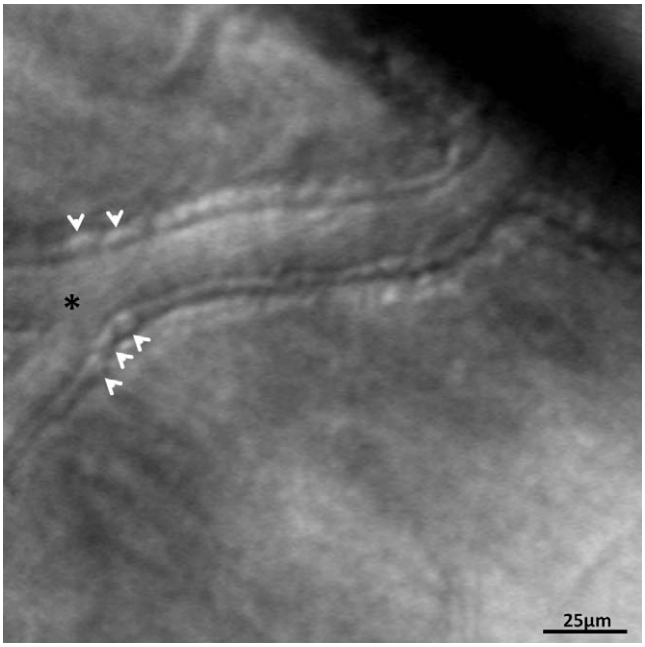

FIGURE 4. Relatively larger mural cells (*white arrows*) around the region of bifurcation in a precapillary arteriole with a lumen diameter of 20 μm. *Asterisk* indicates the point of bifurcation. Image has been contrast stretched for display purposes.

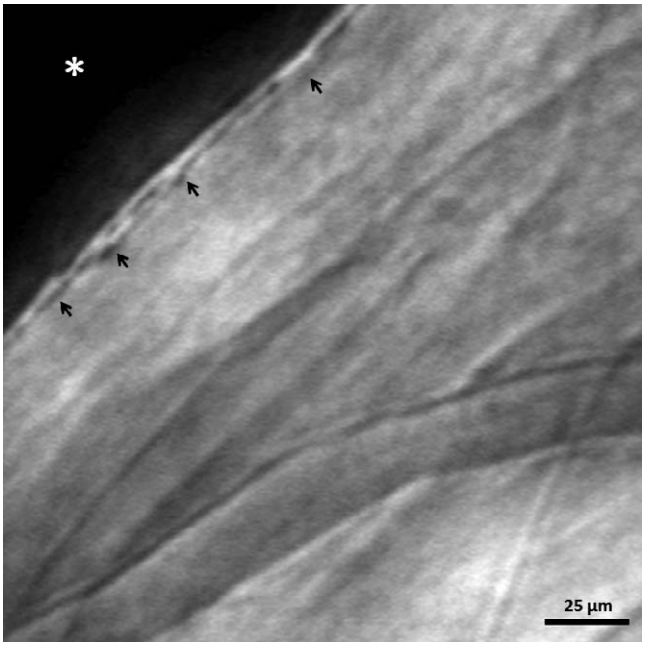

FIGURE 5. Wall structure of a 110-μm lumen diameter venule located 1° above the optic disk. Mural cells (*black arrows*) appeared as flat and elongated in shape. *Asterisk* indicates the lumen of the venule. Image has been contrast stretched for display purposes.

lamina was also formed with distinct cells (Fig. 2A3, white arrows) lined up along the inner side of the blood vessel wall, which was clearly separated from the moving erythrocytes within the vessel lumen. The inner and outer laminae were separated by a thin, dark middle layer (Fig. 2A3). For the arterioles of groups 2 and 3, only one crenulated layer was identified (Figs. 2B3, 2C3, black arrows). Also note that the capillary free zone adjacent to the arterial wall was readily visualized on the perfusion maps as shown in the middle column of Figure 2 (asterisks). The lateral extent of the capillary free zone decreased with decreasing arteriolar lumen diameter as expected. The overall appearances as well as the difference between the appearances of vessel walls for each group were consistent in all eight tested subjects.

While we did not systematically investigate changes in vascular walls between veins and arteries, nor with spatial position relative to bifurcations of vessels, a few generalizations were possible. Relatively larger mural cells were found around the region of arteriolar bifurcation. Figure 4 shows the region of bifurcation in a precapillary arteriole with a lumen diameter of 20 μm in a 51-year-old female. Venular wall structure is relatively thinner when compared with arterioles with similar diameter. Figure 5 shows the venular wall structure of a 110-μm lumen diameter venule located 1° above the optic disk. Typically, the mural cells around venules appeared as flat and elongated in shape when compared with the mural cells in arterioles with comparable lumen diameter and were more difficult to image.

DISCUSSION

Our results demonstrated that the use of an AOSLO with a large displaced aperture allows direct, noninvasive visualization of specializations along the retinal vascular walls. In the following sections of the discussion we cover the relation between our in vivo imaging results and the reported ex vivo structure of the retinal vascular walls.

Vascular Smooth Muscle Cells and Endothelial Cells in Group 1 Vessels

It is well known that blood vessel walls are composed of two types of cells, endothelial cells and mural cells. While the inner wall lining is tiled with endothelial cells, the outer wall lining is formed by pericytes in smaller vessels or vascular smooth muscle cells (vSMCs)[50,51] in larger vessels. Previous electron microscopic studies as well as vessel digests of rat retinal vessels show that the outer vessel wall is composed of continuous single or multiple layers of vSMCs in larger retinal arterioles.[52,53] Shown in Figure 6 (right panel) is a photomicrograph of an untreated retinal arteriole in Sprague-Dawley rat imaged by McGahon et al.[53] The irregular wall thickness formed by a single layer of vSMCs resembles our in vivo arteriolar wall images in the vessels of groups 1, 2, and 3 (Figs. 2A1, 2B1, 2C1). Prior histologic studies have also suggested that the inner endothelial cells and the outer vSMCs are not in direct contact with each other; instead, they are separated by a thin basement membrane.[54] Similarly, our in vivo imaging findings show that for the larger group 1 arterioles, the arteriolar walls appear to have two distinct layers of cell-like structures arranged continuously along the walls separated by a thin, dark, middle layer possibly corresponding to the basement membrane (Fig. 2A3). This correspondence is quite good with previously published descriptions. Quantitative comparisons of our data to the histopathologic literature are difficult. Armulik et al.[55] have pointed out the variability in appearance of the pericytes, and also that while pericyte coverage of the abluminal endothelial surface is almost complete,[56] the actual pericyte to endothelial cell nuclear ratios appear to be approximately 0.5 in human retinal capillaries,[57] but our inability to quantify endothelial cell

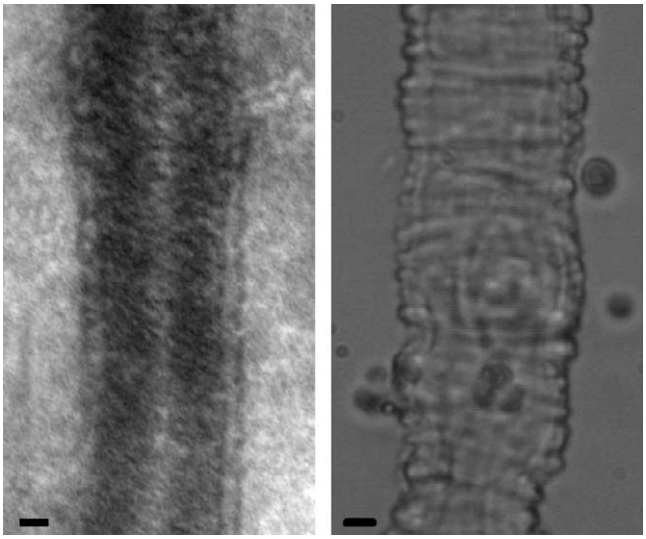

FIGURE 6. Comparison of retinal arteriole images obtained using a dark field AOSLO in human (*left panel*; *scale bar*: 10 μm) and ex vivo photomicrograph in Sprague-Dawley rat[53] (*right panel*; *scale bar*: 5 μm). Image on the *left* has been contrast stretched for display purposes. Image on the *right* was reproduced with permission from the Association for Research in Vision and Ophthalmology.

density precludes comparison of our data to the histology with regard to cell nuclear ratios.

Pericytes in Arterioles and Venules

From histology it is clear that the structure of the arteriolar walls changes systematically for arterioles with different lumen diameters. Toward the smaller vessels there are no vSMCs, but rather pericytes become the major outer portion of the vascular walls.[55,58] In general, pericytes possess a prominent cell body with smaller primary and secondary processes running along and wrapping circumferentially around the blood vessels. Unlike vSMCs in larger vessels, pericytes are embedded within the basement membrane in smaller vessels,[59] showing numerous direct and focal contacts with the endothelial cells through gaps in the basement membrane.[60,61] Pericytes vary substantially in shape and number across different sized blood vessels.[55] For moderate and small sized arterioles they appear as long slender polymorphic cells with a prominent cell body located on the outer wall of the blood vessel. We see this type of transition in the appearance of the vascular walls from group 1 to group 3 vessels in our in vivo imaging (Figs. 2A3, 2B3, 2C3). Also consistent with histology,[58,62] there are morphologic differences among pericytes on the arterial (Fig. 2A3) and venous (Fig. 5) sides of blood vessels imaged using our AOSLO technique. According to our results, pericytes on venules, compared with those of arterioles with similar lumen diameter, tend to be longer, thinner, and flatter (Fig. 5). The number of pericytes varies significantly depending on the type of vessel and lumen diameter. While the correspondences between the in vivo imaging and previous histologic studies are good the exact equivalence is difficult to confirm. For the human data we are using unstained, living tissue, and most studies have used postmortem, stained tissue. In addition, our resolution is limited by the numerical aperture of the human eye, and so the resolution is limited to a little less than 2 μm for our imaging wavelength. Nevertheless, we believe the correspondences are good, and this supports the conclusion that we are imaging mural cells in the living human retina.

Visibility of the Vascular Walls and the Mechanism Generating Optical Contrast

In our study, we did not regularly see the walls of the venules or capillaries, although occasionally we could measure the venule walls and detected hints of capillary walls. In addition the appearance of the vascular walls is more like a longitudinal cross section on our AOSLO images, whereas in reality we know the vessels are cylinders with the mural cells wrapping around the circumference of the vessels (this can be seen in the histology of Fig. 6, right panel). In practice, we do see hints of these circumferential bands as shown in Figures 2C3 and 6, left panel. However, we do not always see these though they must be present. Similarly, for the capillaries and venules we occasionally see hints of mural cells, but not reliably enough to quantify. The lack of visibility of venule and capillary pericytes could be due to their different structure. Capillary pericytes tend to be more rounded than on the precapillary arterioles[55] and on venules they are flattened against the endothelial cells. This raises the issue of what is limiting the detection in our imaging approach. The first issue is resolution. While we are essentially diffraction limited,[63] the structures we are imaging represent small variations in the index of refraction, but they are larger than the approximately 2-μm resolution limit for our imaging system. The second limitation is contrast, and issues here could arise either from the structure of the capillaries, the optical detection approach, or both. Because of the nature of the neurovascular unit the pericyte on capillaries is largely enveloped by the astrocyte endfeet,[55,56] which from our purposes of visualization likely decreases the contrast resulting in the smooth capillary walls we image. The optical limitations arise from the observation that we are using an approach that detects the vascular walls based on forward scatter that is in turn scattered back toward the pupil.[27] This imaging approach is closely related to phase contrast microscopy.[64] Like other methods sensitive to light scattering in retinal imaging,[24,65–68] the degree that the light beam interacts with the tissue is spatially limited. As the imaging beam passes over the vessels the first time, some of the light is diffracted at the vascular wall due to the change in refractive index. While the angle of diffraction is related to the spatial frequency of the wall structure, the amount of light diffracted is related to the total refractive index difference and the axial dimension of the structure within the focal volume. Imaging the vascular wall then becomes an issue of detecting this light that has been diffracted at an angle from the vessel and then scattered back toward the pupil.[27] Because we use a large displaced aperture, the AOSLO has a large depth of field. This means that we have a very large background signal, which arises from the out of focus elements of the retina and a relatively small signal from the vessel structure. We obtain contrast from the plane of focus because it is only here that the illumination beam is compact and a phase structure (the blood vessels) will interact with a significant proportion of the impinging light and therefore be diffracted; thus, whereas the amount of light diffracted is relatively small, the contribution of the nondiffracted light is large. The result is that the high frequency information from the larger vessel walls can be detected but the small amount from capillaries cannot be detected. The reason for not seeing the venule and capillary walls then becomes an issue of signal-to-noise ratio, and suggests that schemes to improve the detection of small signals on a large background, including real time background subtraction or suppression may enable further advances in vascular wall imaging.

Capillary Free Zone

Retinal arteriolar capillary free zone is clearly visible in the arterioles of groups 1 through 3 as shown in the perfusion maps (Figs. 2, 3, middle columns). It has been shown that the width of the periarteriolar capillary free zone increases with increasing oxygen exposure in kitten retinas,[69] and our results show this region decreasing as the diameter of the vessels decrease.

Future Studies and Limitations

One of the main goals of this study was to investigate the possibility of making direct, noninvasive measurements of vascular cells. The ability to make these measurements raises the possibility of examining changes in early diabetes. It is well established that changes to the walls of retinal vessels occurs early in diabetic retinopathy.[36–38] It is often presumed that prevention of the earliest events in the pathogenesis of diabetic retinopathy, such as pericyte loss and microaneurysm development, will prevent the progression of diabetic retinopathy. Our noninvasive imaging approach could provide a unique opportunity to detect and monitor subtle vascular pathologic changes in diabetes over time such as microaneurysm formation, mural cells loss forming resultant pericyte "ghosts" and possibly development of intraretinal microvascular anomalies. It is to be hoped that this may lead to more effective individualized treatment plans and earlier measurements of the efficacy of medical interventions for diabetic retinopathy. Other systemic diseases such as hypertension could produce quantifiable effects on the retinal vascular walls and many other ocular conditions (e.g., vein occlusions) have some involvement of the retinal vasculature.

We have now shown that this type of imaging is possible in a sequential series of healthy subjects, but we have not yet established the reliability and reproducibility for clinical imaging. Further investigations are needed to confirm the retinal vascular wall features presented in this study. Ultimately a direct comparison between in vivo mural cells imaging and histology on the same sample is necessary. Our displaced aperture imaging approach has several limitations. (1) We are not able to resolve pericytes and endothelial cells in capillaries due to our system resolution limit, (2) aperture displacement orientation limits the visibility of both sides of the vascular wall simultaneously though pilot experiments with an annular aperture indicate that this is not a fundamental difficulty, and (3) our AOSLO images primarily show the longitudinal cross section of the blood vessels and, therefore, does not allow complete quantification of mural cell and endothelial cell density.

Conclusions

The current study has led to a new capability for AOSLO imaging: in vivo fine structure of retinal microvascular vessel wall imaging. Our results show that blood vessels mural cells can be readily resolved in healthy subjects for arterioles with a lumen diameter greater than or equal to 10 μm and in major venules. Our noninvasive imaging technique has the potential to detect and monitor vascular morphologic changes in retinal vascular diseases such as diabetic retinopathy, allowing for studies of the structural and functional consequences of vasculopathy.

Acknowledgments

The authors thank Tracy Nguyen and Douglas Horner for the aid in screening subjects, and Dean A. VanNasdale for his helpful discussion.

Supported by National Institutes of Health Grants R01-EY14375, R01-EY07624, R01-EY04395, and Vision Science Core Grant P30EY019008.

Disclosure: **T.Y.P. Chui**, None; **T.J. Gast**, None; **S.A. Burns**, None

References

1. Liang J, Williams DR, Miller DT. Supernormal vision and high-resolution retinal imaging through adaptive optics. *J Opt Soc Am A Opt Image Sci Vis*. 1997;14:2884–2892.
2. Roorda A. Adaptive optics ophthalmoscopy. *J Refract Surg*. 2000;16:S602–607.
3. Le Gargasson JF, Glanc M, Lena P. Retinal imaging with adaptive optics. *Comptes Rendus De L'Académie Des Sciences Serie IV Physique Astrophysique*. 2001;2:1131–1138.
4. Roorda A, Romero-Borja F, Donnelly III W, Queener H, Hebert T, Campbell M. Adaptive optics scanning laser ophthalmoscopy. *Opt Express*. 2002;10:405–412.
5. Zawadzki RJ, Jones SM, Olivier SS, et al. Adaptive-optics optical coherence tomography for high-resolution and high-speed 3D retinal in vivo imaging. *Opt Express*. 2005;13:8532–8546.
6. Zhang Y, Rha J, Jonnal R, Miller D. Adaptive optics parallel spectral domain optical coherence tomography for imaging the living retina. *Opt Express*. 2005;13:4792–4811.
7. Burns SA, Tumbar R, Elsner AE, Ferguson D, Hammer DX. Large-field-of-view, modular, stabilized, adaptive-optics-based scanning laser ophthalmoscope. *J Opt Soc Am A Opt Image Sci Vis*. 2007;24:1313–1326.
8. Pallikaris A, Williams DR, Hofer H. The reflectance of single cones in the living human eye. *Invest Ophthalmol Vis Sci*. 2003;44:4580–4592.
9. Choi SS, Doble N, Lin J, Christou J, Williams DR. Effect of wavelength on in vivo images of the human cone mosaic. *J Opt Soc Am A Opt Image Sci Vis*. 2005;22:2598–2605.
10. Chui TY, Song H, Burns SA. Individual variations in human cone photoreceptor packing density: variations with refractive error. *Invest Ophthalmol Vis Sci*. 2008;49:4679–4687.
11. Chui TY, Song H, Burns SA. Adaptive-optics imaging of human cone photoreceptor distribution. *J Opt Soc Am A Opt Image Sci Vis*. 2008;25:3021–3029.
12. Dubra A, Sulai Y, Norris JL, et al. Noninvasive imaging of the human rod photoreceptor mosaic using a confocal adaptive optics scanning ophthalmoscope. *Biomed Opt Express*. 2011;2:1864–1876.
13. Brainard DH, Roorda A, Yamauchi Y, et al. Functional consequences of the relative numbers of L and M cones. *J Opt Soc Am A Opt Image Sci Vis*. 2000;17:607–614.
14. Hofer H, Carroll J, Neitz J, Neitz M, Williams DR. Organization of the human strichromatic cone mosaic. *J Neurosci*. 2005;25:9669–9679.
15. Putnam NM, Hofer HJ, Doble N, Chen L, Carroll J, Williams DR. The locus of fixation and the foveal cone mosaic. *J Vis*. 2005;5:632–639.
16. Choi SS, Doble N, Hardy JL, et al. In vivo imaging of the photoreceptor mosaic in retinal dystrophies and correlations with visual function. *Invest Ophthalmol Vis Sci*. 2006;47:2080–2092.
17. Duncan JL, Zhang Y, Gandhi J, et al. High-resolution imaging with adaptive optics in patients with inherited retinal degeneration. *Invest Ophthalmol Vis Sci*. 2007;48:3283–3291.
18. Roorda A, Zhang Y, Duncan JL. High-resolution in vivo imaging of the RPE mosaic in eyes with retinal disease. *Invest Ophthalmol Vis Sci*. 2007;48:2297–2303.
19. Carroll J, Choi SS, Williams DR. In vivo imaging of the photoreceptor mosaic of a rod monochromat. *Vision Res*. 2008;48:2564–2568.

20. Carroll J, Dubra A, Gardner JC, et al. The effect of cone opsin mutations on retinal structure and the integrity of the photoreceptor mosaic. *Invest Ophthalmol Vis Sci*. 2012;53: 8006–8015.
21. Takayama K, Ooto S, Hangai M, et al. High-resolution imaging of the retinal nerve fiber layer in normal eyes using adaptive optics scanning laser ophthalmoscopy. *PLoS One*. 2012;7: e33158.
22. Gray DC, Merigan W, Wolfing JI, et al. In vivo fluorescence imaging of primate retinal ganglion cells and retinal pigment epithelial cells. *Opt Express*. 2006;14:7144–7158.
23. Morgan JI, Dubra A, Wolfe R, Merigan WH, Williams DR. In vivo autofluorescence imaging of the human and macaque retinal pigment epithelial cell mosaic. *Invest Ophthalmol Vis Sci*. 2009;50:1350–1359.
24. Scoles D, Sulai YN, Dubra A. In vivo dark-field imaging of the retinal pigment epithelium cell mosaic. *Biomed Opt Express*. 2013;4:1710–1723.
25. Tam J, Martin JA, Roorda A. Noninvasive visualization and analysis of parafoveal capillaries in humans. *Invest Ophthalmol Vis Sci*. 2010;51:1691–1698.
26. Chui TY, Zhong Z, Song H, Burns SA. Foveal avascular zone and its relationship to foveal pit shape. *Optom Vis Sci*. 2012; 89:602–610.
27. Chui TY, Vannasdale DA, Burns SA. The use of forward scatter to improve retinal vascular imaging with an adaptive optics scanning laser ophthalmoscope. *Biomed Opt Express*. 2012;3: 2537–2549.
28. Tam J, Dhamdhere KP, Tiruveedhula P, et al. Subclinical capillary changes in non-proliferative diabetic retinopathy. *Optom Vis Sci*. 2012;89:E692–703.
29. Martin JA, Roorda A. Direct and noninvasive assessment of parafoveal capillary leukocyte velocity. *Ophthalmology*. 2005; 112:2219–2224.
30. Zhong Z, Petrig BL, Qi X, Burns SA. In vivo measurement of erythrocyte velocity and retinal blood flow using adaptive optics scanning laser ophthalmoscopy. *Opt Express*. 2008;16: 12746–12756.
31. Tam J, Roorda A. Speed quantification and tracking of moving objects in adaptive optics scanning laser ophthalmoscopy. *J Biomed Opt*. 2011;16:036002.
32. Zhong Z, Song H, Chui TY, Petrig BL, Burns SA. Noninvasive measurements and analysis of blood velocity profiles in human retinal vessels. *Invest Ophthalmol Vis Sci*. 2011;52:4151–4157.
33. Zhong Z, Huang G, Chui TY, Petrig BL, Burns SA. Local flicker stimulation evokes local retinal blood velocity changes. *J Vis*. 2012;12:3.
34. Ikram MK, Cheung CY, Lorenzi M, Klein R, Jones TL, Wong TY. Retinal vascular caliber as a biomarker for diabetes microvascular complications. *Diabetes Care*. 2013;36:750–759.
35. Kempen JH, O'Colmain BJ, Leske MC, et al. The prevalence of diabetic retinopathy among adults in the United States. *Arch Ophthalmol*. 2004;122:552–563.
36. Mizutani M, Kern TS, Lorenzi M. Accelerated death of retinal microvascular cells in human and experimental diabetic retinopathy. *J Clin Invest*. 1996;97:2883–2890.
37. Li W, Yanoff M, Liu X, Ye X. Retinal capillary pericyte apoptosis in early human diabetic retinopathy. *Chin Med J (Engl)*. 1997; 110:659–663.
38. Joussen AM, Poulaki V, Le ML, et al. A central role for inflammation in the pathogenesis of diabetic retinopathy. *FASEB J*. 2004;18:1450–1452.
39. Avery RL, Pearlman J, Pieramici DJ, et al. Intravitreal bevacizumab (Avastin) in the treatment of proliferative diabetic retinopathy. *Ophthalmology*. 2006;1695.e1–15.
40. Nelson DA, Burgansky-Eliash Z, Barash H, et al. High-resolution wide-field imaging of perfused capillaries without the use of contrast agent. *Clin Ophthalmol*. 2011;5:1095–1106.
41. Kim DY, Fingler J, Werner JS, Schwartz DM, Fraser SE, Zawadzki RJ. In vivo volumetric imaging of human retinal circulation with phase-variance optical coherence tomography. *Biomed Opt Express*. 2011;2:1504–1513.
42. Zotter S, Pircher M, Torzicky T, et al. Visualization of microvasculature by dual-beam phase-resolved Doppler optical coherence tomography. *Opt Express*. 2011;19:1217–1227.
43. Makita S, Jaillon F, Yamanari M, Yasuno Y. Dual-beam-scan Doppler optical coherence angiography for birefringence-artifact-free vasculature imaging. *Opt Express*. 2012;20:2681–2692.
44. Bedggood P, Metha A. Direct visualization and characterization of erythrocyte flow in human retinal capillaries. *Biomed Opt Express*. 2012;3:3264–3277.
45. Pinhas A, Dubow M, Shah N, et al. In vivo imaging of human retinal microvasculature using adaptive optics scanning light ophthalmoscope fluorescein angiography. *Biomed Opt Express*. 2013;4:1305–1317.
46. Ferguson RD, Zhong Z, Hammer DX, et al. Adaptive optics scanning laser ophthalmoscope with integrated wide-field retinal imaging and tracking. *J Opt Soc Am A Opt Image Sci Vis*. 2010;27:A265–277.
47. American National Standard Institute. *American National Standard for Safe Use of Lasers ANSI Z1361–2007*. Orlando, FL: The Laser Institute of America; 2007.
48. Elsner AE, Weber A, Cheney MC, VanNasdale DA, Miura M. Imaging polarimetry in patients with neovascular age-related macular degeneration. *J Opt Soc Am A Opt Image Sci Vis*. 2007;24:1468–1480.
49. Huang G, Zhong Z, Zou W, Burns SA. Lucky averaging: quality improvement of adaptive optics scanning laser ophthalmoscope images. *Opt Lett*. 2011;36:3786–3788.
50. Rouget C. Mémoire sur le dévelopement, la structure et les propriétés physiologiques des capillaries sanguins et lymphatiques. *Arch Physiol Norm Pathol*. 1875;5:603–663.
51. Zimmermann KW. Der feinere Bau der Blutcapillaren. *Z Anat Entwicklungsgesch*. 1923;68:3–109.
52. Hughes S, Chan-Ling T. Characterization of smooth muscle cell and pericyte differentiation in the rat retina in vivo. *Invest Ophthalmol Vis Sci*. 2004;45:2795–2806.
53. McGahon MK, Dawicki JM, Scholfield CN, McGeown JG, Curtis TM. A-type potassium current in retinal arteriolar smooth muscle cells. *Invest Ophthalmol Vis Sci*. 2005;46: 3281–3287.
54. Gerhardt H, Betsholtz C. Endothelial-pericyte interactions in angiogenesis. *Cell Tissue Res*. 2003;314:15–23.
55. Armulik A, Genove G, Betsholtz C. Pericytes: developmental, physiological, and pathological perspectives, problems, and promises. *Dev Cell*. 2011;21:193–215.
56. Mathiisen TM, Lehre KP, Danbolt NC, Ottersen OP. The perivascular astroglial sheath provides a complete covering of the brain microvessels: an electron microscopic 3D reconstruction. *Glia*. 2010;58:1094–1103.
57. Frank RN, Turczyn TJ, Das A. Pericyte coverage of retinal and cerebral capillaries. *Invest Ophthalmol Vis Sci*. 1990;31:999–1007.
58. Cleaver O, Melton DA. Endothelial signaling during development. *Nat Med*. 2003;9:661–668.
59. Mandarino LJ, Sundarraj N, Finlayson J, Hassell HR. Regulation of fibronectin and laminin synthesis by retinal capillary endothelial cells and pericytes in vitro. *Exp Eye Res*. 1993; 57:609–621.

Investigative Ophthalmology & Visual Science

60. Tilton RG, Kilo C, Williamson JR. Pericyte-endothelial relationships in cardiac and skeletal muscle capillaries. *Microvasc Res*. 1979;18:325–335.
61. Cuevas P, Gutierrez-Diaz JA, Reimers D, Dujovny M, Diaz FG, Ausman JI. Pericyte endothelial gap junctions in human cerebral capillaries. *Anat Embryol (Berl)*. 1984;170:155–159.
62. Ikebe T, Shimada T, Ina K, Kitamura H, Nakatsuka K. The three-dimensional architecture of retinal blood vessels in KK mice, with special reference to the smooth muscle cells and pericytes. *J Electron Microsc (Tokyo)*. 2001;50:125–132.
63. Zou W, Qi X, Burns SA. Woofer-tweeter adaptive optics scanning laser ophthalmoscopic imaging based on Lagrange-multiplier damped least-squares algorithm. *Biomed Opt Express*. 2011;2:1986–2004.
64. Ford TN, Chu KK, Mertz J. Phase-gradient microscopy in thick tissue with oblique back-illumination. *Nat Methods*. 2012;9:1195–1197.
65. Elsner AE, Burns SA, Weiter JJ, Delori FC. Infrared imaging of sub-retinal structures in the human ocular fundus. *Vision Res*. 1996;36:191–205.
66. Hartnett ME, Elsner AE. Characteristics of exudative age-related macular degeneration determined in vivo with confocal and indirect infrared imaging. *Ophthalmology*. 1996;103:58–71.
67. Elsner A, Miura M, Burns S, et al. Multiply scattered light tomography and confocal imaging: detecting neovascularization in age-related macular degeneration. *Opt Express*. 2000;7:95–106.
68. Diniz B, Ribeiro RM, Rodger DC, Maia M, Sadda S. Drusen detection by confocal aperture-modulated infrared scanning laser ophthalmoscopy. *Br J Ophthalmol*. 2013;97:285–290.
69. Phelps DL. Oxygen and developmental retinal capillary remodeling in the kitten. *Invest Ophthalmol Vis Sci*. 1990;31:2194–2200.

Investigative Ophthalmology & Visual Science